BMP gradients steer nerve growth cones by a balancing act of LIM kinase and Slingshot phosphatase on ADF/cofilin

Zhexing Wen,[1] Liang Han,[1] James R. Bamburg,[2,3] Sangwoo Shim,[4] Guo-li Ming,[4] and James Q. Zheng[1]

[1]Department of Neuroscience and Cell Biology, University of Medicine and Dentistry of New Jersey, Robert Wood Johnson Medical School, Piscataway, NJ 08854
[2]Department of Biochemistry and Molecular Biology and [3]Molecular, Cellular, and Integrative Neuroscience Program, Colorado State University, Fort Collins, CO 80523
[4]Institute for Cell Engineering, Department of Neurology, Johns Hopkins University School of Medicine, Baltimore, MD 21205

Bone morphogenic proteins (BMPs) are involved in axon pathfinding, but how they guide growth cones remains elusive. In this study, we report that a BMP7 gradient elicits bidirectional turning responses from nerve growth cones by acting through LIM kinase (LIMK) and Slingshot (SSH) phosphatase to regulate actin-depolymerizing factor (ADF)/cofilin-mediated actin dynamics. *Xenopus laevis* growth cones from 4–8-h cultured neurons are attracted to BMP7 gradients but become repelled by BMP7 after overnight culture. The attraction and repulsion are mediated by LIMK and SSH, respectively, which oppositely regulate the phosphorylation-dependent asymmetric activity of ADF/cofilin to control the actin dynamics and growth cone steering. The attraction to repulsion switching requires the expression of a transient receptor potential (TRP) channel TRPC1 and involves Ca^{2+} signaling through calcineurin phosphatase for SSH activation and growth cone repulsion. Together, we show that spatial regulation of ADF/cofilin activity controls the directional responses of the growth cone to BMP7, and Ca^{2+} influx through TRPC tilts the LIMK-SSH balance toward SSH-mediated repulsion.

Introduction

Wiring of the intricate nervous system requires guided axonal growth to form specific neuronal connections. Motile growth cones at the tip of elongating axons sense spatiotemporally distributed guidance cues to steer through the complex environment to reach the correct targets. A variety of attractive and repulsive guidance molecules and their corresponding receptors have now been identified (Tessier-Lavigne and Goodman, 1996; Dickson, 2002). Recent studies also show that several classic morphogens, including the Hedgehog, Wingless/Wnt, and Bone Morphogenic Protein (BMP)/TGFβ families, play a key role in axon guidance (Charron and Tessier-Lavigne, 2005). During neural tube development, several members of the BMP/TGFβ family, such as BMP7, GDF7, and BMP6, are expressed in the dorsal roof plate, and it is believed that their main function is to control the induction and differentiation of dorsal interneurons (Lee and Jessell, 1999; Liu and Niswander, 2005). Interestingly, BMP7 at the roof plate was recently shown to exhibit a chemorepellent function in the initial trajectory of commissural axons in the developing spinal cord (Augsburger et al., 1999; Butler and Dodd, 2003). However, a generalized role for BMP molecules in growth cone motility and guidance has not been established. Little is also known about the signaling mechanisms underlying BMP guidance effects. The canonical BMP–TGFβ pathway controls neuronal cell fate and involves activation of the Smad transcription factors (Feng and Derynck, 2005), but this long-term transcription-dependent signaling is unlikely to be involved in rapid growth cone responses to BMP7 (Augsburger et al., 1999). Rather, the cytoskeletal dynamics controlling growth cone motility is expected to be targeted by BMP7 to generate specific guidance responses (Yoshikawa and Thomas, 2004; Bovolenta, 2005).

In this study, we used cultured embryonic *Xenopus laevis* spinal neurons and a well-established turning assay to investigate the cellular mechanisms underlying BMP7 guidance. We report that a BMP7 gradient elicits bidirectional turning responses of *Xenopus* growth cones in culture. *Xenopus* growth cones were initially attracted to a BMP7 gradient 4–8 h after plating but became repelled by BMP7 after overnight culture (20–24 h).

Z. Wen and L. Han contributed equally to this paper.

Correspondence to James Q. Zheng: james.zheng@umdnj.edu

Abbreviations used in this paper: ADF, actin-depolymerizing factor; ANOVA, analysis of variance; BMP, Bone Morphogenic Protein; CaN, calcineurin; DN, dominant negative; DTAF, 5-(4,6-dichlorotriazinyl)aminofluorescein; IF, immunofluorescence; LIMK, LIM kinase; p-XAC, phosphorylated XAC; SFM, serum-free medium; SSH, Slingshot; TRP, transient receptor potential; WT, wild type; XAC, *Xenopus* ADF/cofilin.

The online version of this article contains supplemental material.

The Journal of Cell Biology, Vol. 178, No. 1, July 2, 2007 107–119
http://www.jcb.org/cgi/doi/10.1083/jcb.200703055

We further show that LIM kinase (LIMK) and Slingshot (SSH) phosphatase mediate attraction and repulsion, respectively, through the phosphorylation regulation of their common target, actin-depolymerizing factor (ADF)/cofilin. Finally, we demonstrate that the switching of attraction to repulsion results from the emergence of Ca^{2+} signals from a transient receptor potential (TRP) channel (TRPC1) in overnight cultures. The elevated amount of TRPC1 on the growth cone surface of overnight neurons allows Ca^{2+} signaling that activates calcineurin (CaN) phosphatase and SSH, which is dominant over the LIMK activation, to induce repulsion. Thus, these data indicate that BMP7 acts through distinct LIMK and Ca^{2+}–CaN–SSH pathways that converge on ADF/cofilin to locally regulate the actin cytoskeleton and control the direction of growth cone steering.

Results

Bidirectional growth cone responses to BMP7 gradients

To study the guidance effects of BMP molecules, we performed the turning assay on *Xenopus* growth cones in culture (Guirland et al., 2003). We first examined the growth cone responses to the BMP7 gradient in 4–8-h *Xenopus* neuronal cultures. A gradient created by pulsatile ejection of BMP7 at 5 μM (in pipette) induced marked attractive turning of the growth cone toward the pipette (Fig. 1 B), whereas the control solution (without BMP7) had no influence on the direction of growth cone extension (Fig. 1 A). We quantified the turning responses by measuring the turning angle and net extension of each growth cone over a 30-min assay period and summarized the overall responses in means (Fig. 1 E). BMP7 gradients induced attraction at the concentrations of 0.5 or 5 μM in pipette, whereas 0.05 μM BMP7 (in pipette) or the control exerted no directional influence. Based on the previous estimate and fluorescent imaging (Lohof et al., 1992; Zheng et al., 1994), the effective concentrations of BMP7 at the growth cone for eliciting attraction are estimated to be ∼0.5 nM or 5 nM, respectively, which are within the physiological range of BMP molecules reported previously (Lein et al., 1995; Le Roux et al., 1999). Although 5 μM BMP7 in pipette appears to be more effective in inducing attraction, no statistical significance was found between these two groups ($P > 0.5$; Mann-Whitney test). Identical gradients of BMP2, a member of the BMP2/4 subfamily, did not induce any turning responses (Fig. 1 E). Although the mean lengths of growth cone extension varied slightly among different groups (Fig. 1 E), no statistical difference was detected ($P > 0.5$; one-way analysis of variance [ANOVA]). Therefore, BMP7 gradients mainly influenced the direction, not the rate, of growth cone extension.

Xenopus neurons exhibit different responses to certain guidance cues when cultured for different times (Ming et al., 1997; Shewan et al., 2002). Therefore, we examined the turning response to BMP7 in overnight cultures (20–24 h). The same BMP7 gradient (5 μM in pipette) was found to induce marked repulsive turning in overnight neurons (Fig. 1 D), whereas the control exhibited no effect (Fig. 1 C), which was further confirmed by the mean turning angles (Fig. 1 F). Consistently, BMP2 gradients had no influence on overnight growth cones (Fig. 1 F), supporting the notion that BMP7 guidance effects unlikely result from nonspecific actions of BMP molecules. Finally, the net extension of these overnight growth cones was not significantly affected by BMP7 or BMP2 ($P > 0.5$; one-way ANOVA; Fig. 1 F).

To eliminate the possibility that different populations of *Xenopus* neurons were responsible for distinct turning responses, we performed a double turning assay in which the same growth cone was examined at 4–8 h and again at 20–24 h

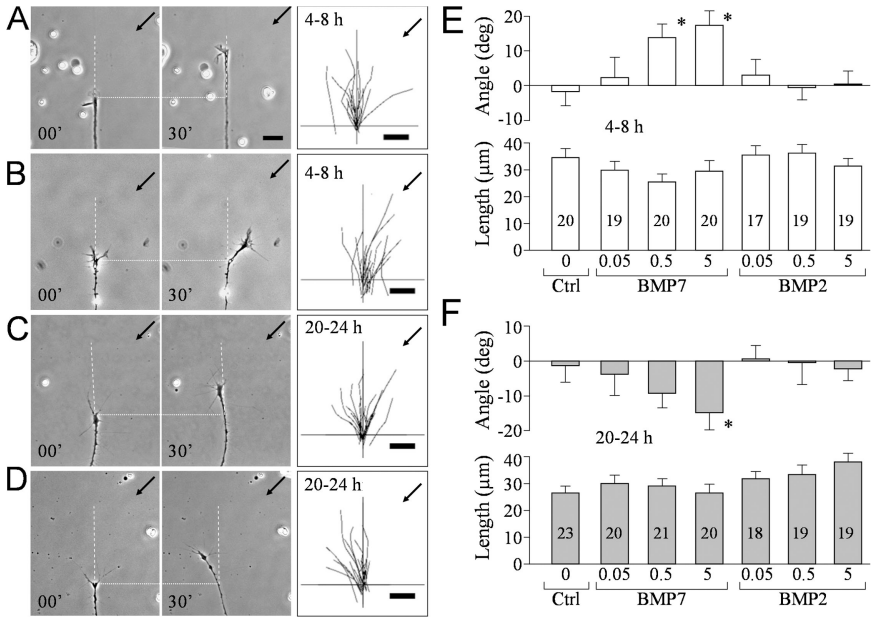

Figure 1. **Bidirectional responses of nerve growth cones to BMP7 at different times in culture.** (A–D) Representative phase-contrast images showing the turning responses of *Xenopus* growth cones from 4–8-h cultures (A and B) or overnight (20–24 h) cultures (C and D) at the onset (0 min) and end of 30 min of exposure to a BMP7 gradient (5 μM in pipette; B and D) or a control saline (A and C). Only the growth cone and part of its adjacent neurite are shown in the image. Scattered yolk granules (small bright objects) are present in each image and can be used as fiduciary markers. Horizontal dotted lines show the position of the growth cone at the onset of the turning assay. Vertical dashed lines show the original trajectory of the growth cone (determined from the growth cone and the adjacent 20 μm of neurite). Arrows indicate the direction of the gradient. Numbers indicate the time after the onset of the gradient. The overall responses of all of the growth cones in each group are depicted by the composite tracings of the trajectory of neurite extension of each growth cone during the 30-min turning assay. The origin is the center of the growth cone at the onset of the gradient, and the original direction of growth cone extension is vertical. (E and F) Mean turning angles (top) and lengths of net growth cone extension (bottom) of different groups of growth cones examined in 4–8-h cultures (E) or 20–24-h cultures (F). BMP concentrations are shown as micromolars in the pipette. The numbers of growth cones examined for each condition are shown on the bars. Asterisks indicate significant differences from the corresponding control (*, $P < 0.05$; Mann-Whitney test). Error bars represent SEM. Bars, 20 μm.

after plating. To track the same growth cone, a special coverslip with etched grids and labels was used (Fig. 2 A). We found that the same growth cone responded to the BMP7 gradient (5 μM in pipette) with marked attraction at 5 h after plating but was repelled by the same BMP7 gradient at 22 h (Fig. 2 A). Of 20 growth cones subjected to the double turning assay, a great majority switched their turning responses from attraction to repulsion overnight, as indicated by the cumulative distribution and the means of turning angles (Fig. 2 B). No significant change in neurite extension was observed ($P > 0.5$; one-way ANOVA; Fig. 2 B). These data demonstrate that the same growth cone exhibits bidirectional responses to BMP7 after different times in culture.

We also examined the BMP7-induced turning responses in the presence of follistatin, an antagonist of BMP7, and noggin, an antagonist of the BMP2/4 subclass (Yamashita et al., 1995; Zimmerman et al., 1996). Bath presence of follistatin, not noggin, eliminated BMP7-induced attraction in 4–8-h neurons (Fig. 2 C) and repulsion in overnight cultures (Fig. 2 D), supporting the notion that BMP7, not BMP2, selectively induces growth cone turning. BMP molecules typically act through BMP receptors I and II (BMPRI and BMPRII), and their kinase activity is responsible for Smad activation and transcription regulation (Feng and Derynck, 2005). *Xenopus* neurons express a long form of BMPRII (Frisch and Wright, 1998), and we have verified it by RT-PCR analysis (Fig. S1 A, available at http://www.jcb.org/cgi/content/full/jcb.200703055/DC1). To evaluate the involvement of BMP receptors in BMP7 guidance, we overexpressed in *Xenopus* spinal neurons a dominant-negative (DN) BMPRII, which lacks the cytoplasmic region (Frisch and Wright, 1998). Blastomere injection of mRNA encoding DN-BMPRII together with FITC-dextran as a cell tracer was used to express DN-BMPRII in *Xenopus* neurons (Alder et al., 1995). We found that both attractive and repulsive turning responses to BMP7 were abolished by the expression of DN-BMPRII but not the wild-type (WT) BMPRII (Fig. 2, C and D).

Unlike other TGFβ type II receptors, BMPRII has a long carboxy tail after the kinase domain, which is not required for BMP activation of the Smad pathway (Ishikawa et al., 1995; Nishihara et al., 2002) but interacts with other signaling pathways (Foletta et al., 2003; Hassel et al., 2004; Lee-Hoeflich et al., 2004; Eaton and Davis, 2005). When we overexpressed a short form of BMPRII lacking the carboxy tail in *Xenopus* neurons, we found that short form BMPRII completely abolished the bidirectional turning responses to BMP7 (Fig. 2, C and D). These data indicate that the BMP7 effects on growth cone turning do not depend on the Smad pathway. This conclusion is consistent with the rapid turning responses to BMP7 gradients (in minutes) and is further supported by the finding that the general transcription inhibitor actinomycin D could not block BMP7-induced attraction in 4–8-h neurons (Fig. 2 C) and repulsion in overnight cultures (Fig. 2 D) when used at a concentration (2.5 μg/ml) that is shown to inhibit [^{3}H]uridine incorporation into RNA in *Xenopus* cultures (O'Dowd, 1983; Stoop and Poo, 1995).

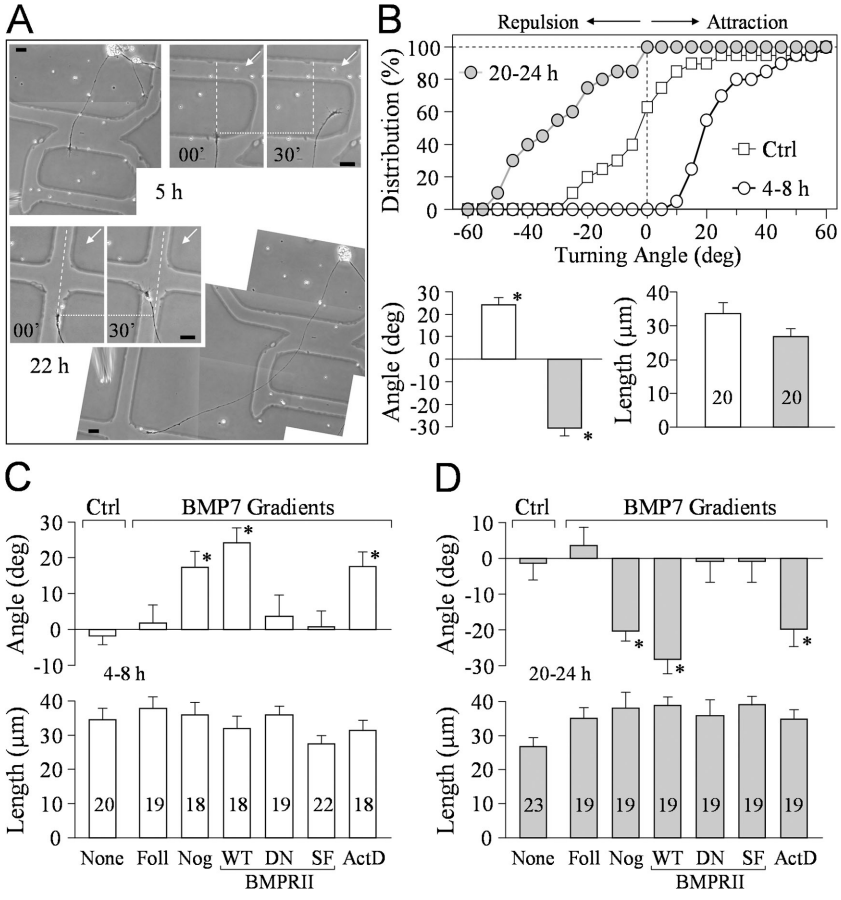

Figure 2. **Double turning responses of the same growth cone at different times and the involvement of BMP receptors.** (A) Representative images showing the turning responses of the same *Xenopus* growth cone at 5 (paired panels on the top right) and 22 h (paired panels at the center left) after plating (5 μM BMP7 in pipette). Dotted lines indicate the corresponding positions of the growth cone at the onset of the turning assay, dashed lines indicate the original directions of growth cone extension, and arrows point to the BMP7 gradient. Irregular-shaped low magnification images were stitched together to show the cell body, its neurites, and its location on the grid. (B) Quantitative analysis of the turning responses from 20 growth cones subjected to the double turning assay. The cumulative histogram in the top panel shows the distribution of the turning angles for these growth cones. Each point represents the percentage of growth cones with final turning angles equal to or less than the values indicated on the abscissa. The control curve is from the 6-h group shown in Fig. 1. The mean turning angles and lengths of growth cone extension from these 20 growth cones are shown in the bottom panel. (C and D) BMPRII mediates BMP7 attraction in 4–8-h cultures (C) and repulsion in overnight cultures (D). The mean turning angles (top) and lengths of growth cone extension (bottom) are shown in the bar graphs. The number of growth cones examined in each group is indicated in the length bar graphs. Asterisks indicate significant differences compared with the corresponding control (*, $P < 0.05$; Mann-Whitney test). Ctrl, control; Foll, follistatin; Nog, noggin; WT, wild type; DN, dominant negative; SF, short form; ActD, actinomycin D. Error bars represent SEM. Bars, 20 μm.

Together, these findings show that BMP7 guidance is mediated by BMP receptors, involves signaling independent of the canonical Smad transcription pathway, and requires the carboxy-terminal regions of BMPRII.

LIMK mediates BMP-induced attraction in 4–8-h cultures

The carboxy tail of BMPRII interacts with LIMK1 in mammals and *Drosophila melanogaster* (Foletta et al., 2003; Lee-Hoeflich et al., 2004; Eaton and Davis, 2005). LIMK1 is a key regulator of the actin cytoskeleton through its phosphorylation of ADF/cofilin at serine-3 for inactivation (Scott and Olson, 2007). A peptide containing the serine-3 sequence of ADF/cofilin (32 amino acids; referred to as the S3 peptide) has been widely used as an effective competitive inhibitor of LIMK1 (Aizawa et al., 2001; Nishita et al., 2002; Heredia et al., 2006). We synthesized the S3 peptide containing the specific *Xenopus* ADF/cofilin (XAC) sequence of the LIMK phosphorylation site as a chimera with a penetratin sequence for uptake into cultured neurons (Prochiantz, 1996). Bath application of 10 μg/ml of the S3 peptide completely blocked growth cone attraction induced by the BMP7 gradient (Fig. 3 B), whereas 10 μg/ml of the control peptide (the reversed sequence of the XAC S3 peptide with the normal penetratin internalization sequence; RV-S3 peptide) did not affect BMP7-induced attraction (Fig. 3 A). The inhibition of BMP7-induced attraction by S3 peptides is clearly depicted by the cumulative distribution of turning angles of all growth cones examined (Fig. 3 E). A majority of growth cones exposed to BMP7 gradients alone or with RV-S3 in bath exhibited positive turning angles, resulting in a marked shift of the angle distribution to the positive territory. However, growth cones treated with S3 peptides did not show a directional preference in response to the BMP7 gradient, resulting in an angle distribution that overlaps with that of the control and centers at zero. The mean turning angles further highlight the effective inhibition of BMP7-induced attractive responses of growth cones by S3 treatment (Fig. 3 F). All of these treatments did not significantly affect the growth cone extension ($P > 0.5$; one-way ANOVA).

We further tested the role of LIMK1 by expressing DN-LIMK1 (Asp 460 replaced with Asn), which is a catalytically dead mutant of LIMK1. Consistent with the S3 results, BMP7-induced growth cone attraction was completely abolished by DN-LIMK1 (Fig. 3 D), whereas WT-LIMK1 had no effect (Fig. 3 C). The overall turning responses of DN-LIMK1–expressing growth cones are similar to those treated with the S3 peptide, both exhibiting a mean turning angle of about zero (Fig. 3, E and F). On the other hand, blocking Ca^{2+} influx by Ca^{2+}-free solution or buffering intracellular Ca^{2+} concentration ($[Ca^{2+}]_i$) by the intracellular loading of BAPTA, a strong Ca^{2+} chelator, did not generate any effect on BMP7-induced attraction. Similarly, inhibition of either Ca^{2+}–calmodulin-dependent kinase II by 5 μM of the specific inhibitor KN93 or inhibition of PKA by 50 μM of a membrane-permeable cAMP antagonist, Rp-cAMPS, did not affect BMP7-induced attraction. Therefore, BMP7-induced attraction is mediated by LIMK and is independent of the Ca^{2+} and cAMP signaling pathways.

BMP7-induced repulsion is mediated by SSH phosphatases

We first tested the involvement of LIMK1 in BMP7-induced repulsion in overnight cultures and found that bath application of S3 or RV-S3 peptides did not affect the repulsion (Fig. 4 A). Similarly, DN-LIMK1 expression did not affect BMP7-induced repulsion (Fig. 4 A). However, the overexpression of WT-LIMK1 was found to abolish the repulsion. Recent studies show that a family of phosphatases, named SSH, dephosphorylate ADF/cofilin at serine-3 to oppose LIMK1 effects on ADF/cofilin activity (Niwa et al., 2002; Endo et al., 2003; Nishita et al., 2005). If SSH mediated the repulsion, its action could have been attenuated by overexpressing LIMK1. To test this possibility,

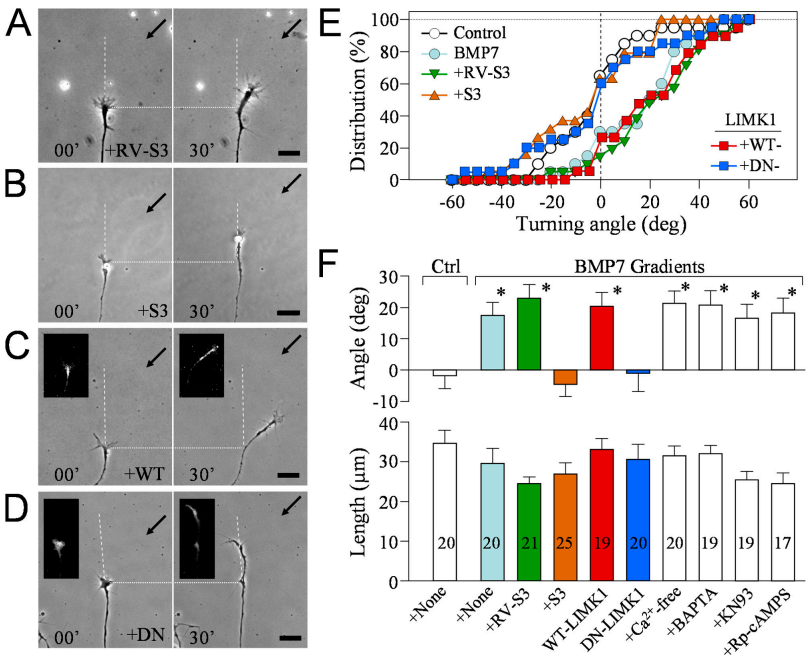

Figure 3. **LIMK mediates BMP7-induced attraction in 4–8-h neurons.** (A and B) Representative images showing *Xenopus* growth cones from 4–8-h cultures at the onset (0 min) and end of a 30-min exposure to a BMP7 gradient (5 μM in pipette) with 10 μg/ml RV-S3 control peptide (A) or 10 μg/ml S3 peptide (B). (C and D) Representative images of growth cones from embryos expressing WT-LIMK1 (C) or DN-LIMK1 (D) at the onset (0 min) and end of a 30-min exposure to a BMP7 gradient (5 μM in pipette). The insets are the corresponding fluorescence of coinjected fixable FITC-dextran. (A–D) Horizontal dotted lines show the positions of the growth cone at the onset of the turning assay, and arrows indicate the direction of the gradient. Dashed lines show the trajectories of the growth cone at the onset of the assay. (E) Cumulative histograms showing the distribution of the turning angles for each condition. Each point represents the percentage of growth cones with final turning angles equal to or less than the values indicated on the abscissa. (F) Mean turning angles (top) and net extension (bottom) of different groups of growth cones examined in 4–8-h cultures. The numbers of growth cones examined for each condition are shown on the bars. For clarity, colors in E and F are matched to represent the same group of growth cones. Asterisks indicate significant differences from the corresponding control (*, $P < 0.01$; Mann-Whitney test). Error bars represent SEM. Bars, 20 μm.

we overexpressed DN-SSH (a phosphatase-defective mutant of *Xenopus* SSH in which the conserved Cys residue in the catalytic pocket is replaced by Ser; Tanaka et al., 2005) in *Xenopus* neurons. Interestingly, growth cones of overnight neurons expressing DN-SSH responded to the BMP7 gradient with marked attraction instead of repulsion, whereas WT-SSH expression did not influence the repulsion (Fig. 4 B). Furthermore, the attraction in overnight neurons overexpressing DN-SSH was blocked by S3 peptides but not RV-S3 (Fig. 4 B). These findings suggest that BMP7 activates both LIMK1 and SSH pathways in overnight neurons, but the SSH pathway dominates to result in repulsion; however, when SSH is inhibited, localized LIMK1 activation takes in charge for attraction. Overall, these results show that BMP7 signals through the LIMK1 and SSH pathways to regulate opposite turning responses and that a balancing act of LIMK1 and SSH controls specific growth cone responses to the BMP7 gradient.

LIMK and SSH target ADF/cofilin to regulate the actin dynamics for bidirectional turning

LIMK1 and SSH oppositely control the activity of ADF/cofilin to regulate the actin cytoskeleton dynamics in neurite outgrowth, cell migration, and polarity (Bamburg, 1999; Gungabissoon and Bamburg, 2003). Phosphorylation of serine-3 of ADF/cofilin inhibits its ability to sever filaments and enhance their subunit turnover. Therefore, BMP7-induced growth cone attraction and repulsion may involve localized ADF/cofilin-mediated stabilization and destabilization of filamentous actin, respectively. Our high resolution live imaging of the actin cytoskeleton in the growth cone appears to support this notion. In 4–8-h neurons, the BMP7 gradient rapidly induced local actin-based protrusions (both lamellipodia and filopodia) on the near side of the growth cone facing BMP7 before the turning of the growth cone shaft (Fig. S2, A and B; and Video 1, available at http://www.jcb.org/cgi/content/full/jcb.200703055/DC1). In overnight cultures, however, a BMP7 gradient elicited a rapid onset of asymmetric protrusion of the actin-based lamellipodia and filopodia on the distal side of the growth cone (with respect to the BMP7 pipette) followed by repulsion (Fig. S2, C and D). At the same time, limited protrusive activity on the BMP7 pipette side of the growth cone was observed, suggesting an inhibition of actin polymerization (Fig. S2 C). The inhibition of protrusive activity was most apparent in the middle of this time-lapse sequence (Video 2).

We next performed quantitative immunofluorescence (IF) microscopy to examine the phosphorylation level of ADF/cofilin in *Xenopus* growth cones exposed to bath application of BMP7 in 4–8-h and overnight cultures. *Xenopus* neurons of 4–8 h exhibited a low level of phosphorylated XAC (p-XAC) in the growth cone (Fig. 5 A), which was markedly increased by 10 min of exposure to 5 nM BMP7. However, the level of p-XAC in the growth cone of overnight cultures was much higher than that of the untreated 4–8-h neurons, which was largely reduced by 5 nM BMP7 (Fig. 5 A). We quantified the intensities of p-XAC and total XAC of all of the growth cones examined and normalized the intensity values against that of the corresponding control group of 4–8-h cultures (Fig. 5 B). The total level of endogenous XAC was not changed by BMP7 and other treatments, but BMP7 induced a substantial increase in the level of p-XAC in 4–8-h neurons and a decrease in overnight neurons. Importantly, the BMP7-induced increase in p-XAC was abolished by the bath application of S3 peptides but not RV-S3, supporting the notion that ADF/cofilin is phosphorylated by LIMK1 in response to BMP7 in 4–8-h neurons. Expression of DN-SSH in the overnight neurons abolished the decrease in the level of p-XAC upon BMP7 exposure and, interestingly, further increased the overall p-XAC in the growth cone (Fig. 5 B). It should be noted that the lack of further elevation of the p-XAC level upon BMP7 exposure in the overnight neurons expressing DN *Xenopus* SSH may reflect the limited sensitivity of quantitative IF in detecting small changes. Finally, the expression of short form BMPRII completely abolished BMP7-induced changes in p-XAC levels in both culture conditions (Fig. 5 B). These data support a model in which BMP7 signaling through BMPRII acts upon LIMK1 to phosphorylate ADF/cofilin in 4–8-h neurons but activates SSH to dephosphorylate ADF/cofilin in overnight neurons.

BMP7 gradients likely regulate ADF/cofilin in a spatially restricted manner to induce distinct turning responses. Using 5-(4,6-dichlorotriazinyl)aminofluorescein (DTAF) as the volume label (Schindelholz and Reber, 1999), we examined the spatial

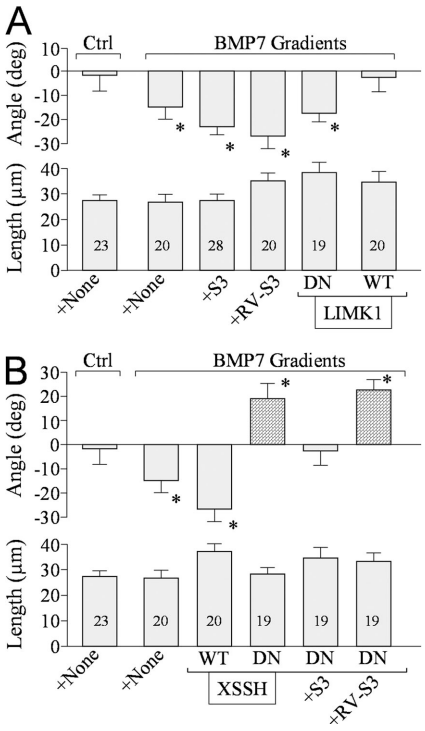

Figure 4. **BMP7-induced repulsion in overnight cultures is mediated by SSH phosphatase.** (A and B) The bar graphs summarize the mean turning angles (top) and net extension (bottom) of different groups of growth cones examined for the involvement of LIMK (A) and SSH (B) in overnight cultures. The numbers of growth cones examined for each condition are indicated on each bar. Asterisks indicate significant differences from the corresponding control (*, $P < 0.05$; Mann-Whitney test). (B) The bars filled with a pattern show the turning responses switched from the original one (repulsion to attraction in this case). Error bars represent SEM.

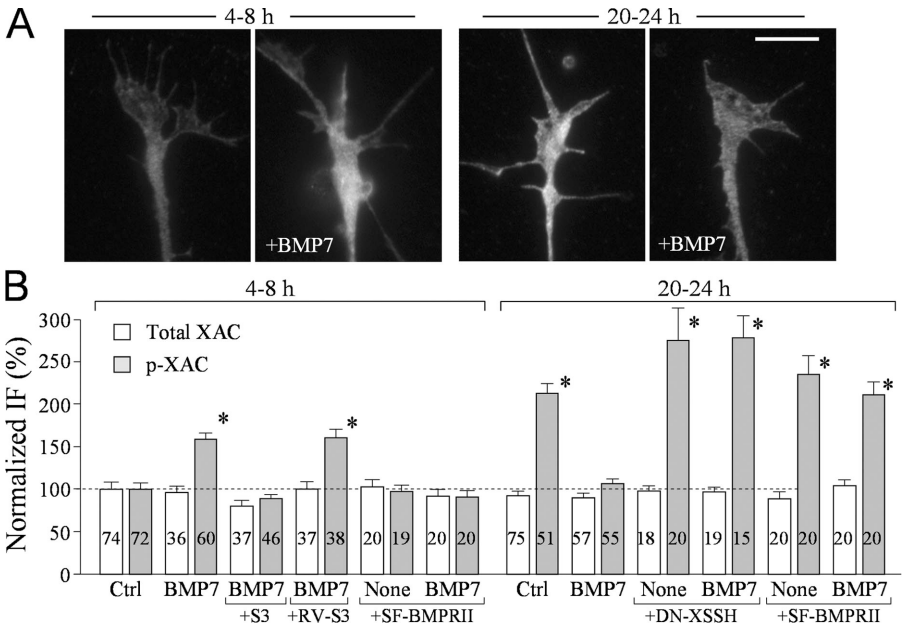

Figure 5. **LIMK and SSH control the phosphorylation of ADF/cofilin in response to BMP7.** (A) Representative fluorescent images of *Xenopus* growth cones of 4–8-h and overnight cultures that were immunostained with a specific antibody against p-XAC without and with bath BMP7 treatment (5 nM for 10 min). (B) Normalized levels of p-XAC and XAC in *Xenopus* growth cones of 4–8-h cultures and overnight cultures with and without bath BMP7 exposure (5 nM for 10 min) under different treatments. The numbers of growth cones examined for each condition are indicated on the bars. Asterisks indicate values that were significantly different from the control (*, $P < 0.01$; *t* test). Error bars represent SEM. Bar, 10 μm.

distribution of p-XAC in response to a BMP7 gradient using ratiometric imaging. We found that a BMP7 gradient induced a preferential increase of p-XAC on the near side of the growth cone facing the BMP7 pipette in 6-h cultures, resulting in an asymmetry of p-XAC (Fig. 6 A). However, the same BMP7 gradient appears to induce a reversed asymmetry of p-XAC in overnight neurons (Fig. 6 A). Similar ratiometric imaging of the total XAC against the volume (DTAF) showed a relatively even distribution upon the BMP7 gradient in both 6-h and overnight cultures. Quantification of the asymmetry using the five-box analysis method (Yao et al., 2006) confirms that a BMP7 gradient induces opposite asymmetries of p-XAC in the 6-h and overnight growth cones, the former with a higher p-XAC level on the near side and the latter with a lower p-XAC level on the near side (Fig. 6 B). Consistently, the distribution of total XAC is uniform with and without BMP7 gradients. Together with the bath application data (Fig. 5), these findings support the notion that a BMP7 gradient induces a local elevation of ADF/cofilin phosphorylation at the near side for attraction in 4–8-h cultures but a local decrease of ADF/cofilin phosphorylation for repulsion in overnight neurons.

To directly assess the functional role of ADF/cofilin phosphorylation in BMP7-induced growth cone guidance, we expressed various forms of XAC in *Xenopus* neurons, including WT-XAC

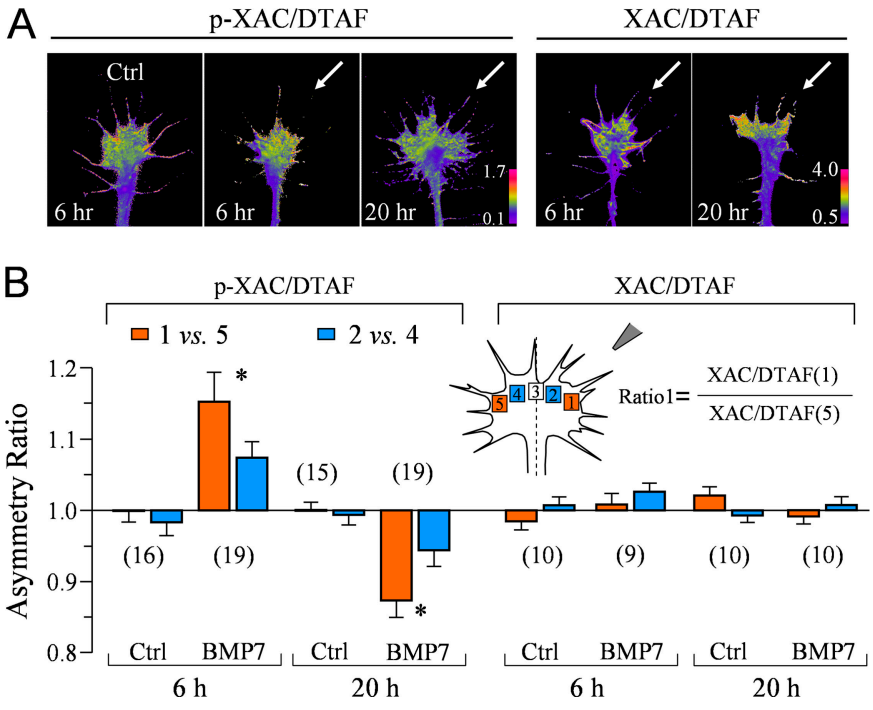

Figure 6. **Spatial pattern of p-XAC in the growth cone exposed to a BMP7 gradient.** (A) Representative ratiometric images of p-XAC/DTAF in a 6-h control growth cone and 6- and 20-h growth cones exposed for 5 min to a BMP7 gradient (arrows). Similar ratiometric images of total XAC/DTAF are also shown on the right. (B) Quantitative measurements of the asymmetry of p-XAC/DTAF and XAC/DTAF using the five-box analysis method. Only the formula for ratio 1 is depicted for simplicity. A ratio close to 1 indicates no asymmetry, a ratio above 1 indicates an asymmetry with the higher level on the near side of the growth cone (close to the pipette), and vice versa. Numbers in parentheses indicate the numbers of growth cones examined for each condition. Asterisks indicate significant differences from the control (*, $P < 0.01$; *t* test). Error bars represent SEM.

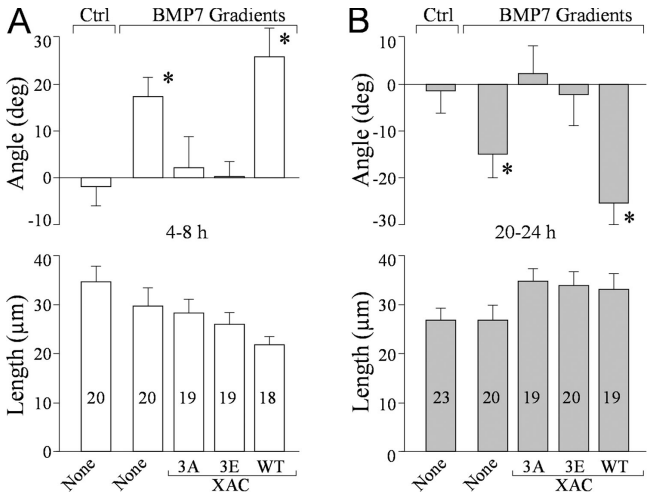

Figure 7. **BMP7-induced bidirectional turning of the growth cones depends on the phosphorylation regulation of ADF/cofilin activity.** (A and B) Mean turning angles (top) and lengths of net extension (bottom) of different groups of the growth cones examined in 4–8-h cultures (A) and overnight cultures (B). Numbers indicate the total numbers of growth cones examined for each condition. Asterisks indicate significant differences from the corresponding control group (*, $P < 0.01$; Mann-Whitney test). Error bars represent SEM.

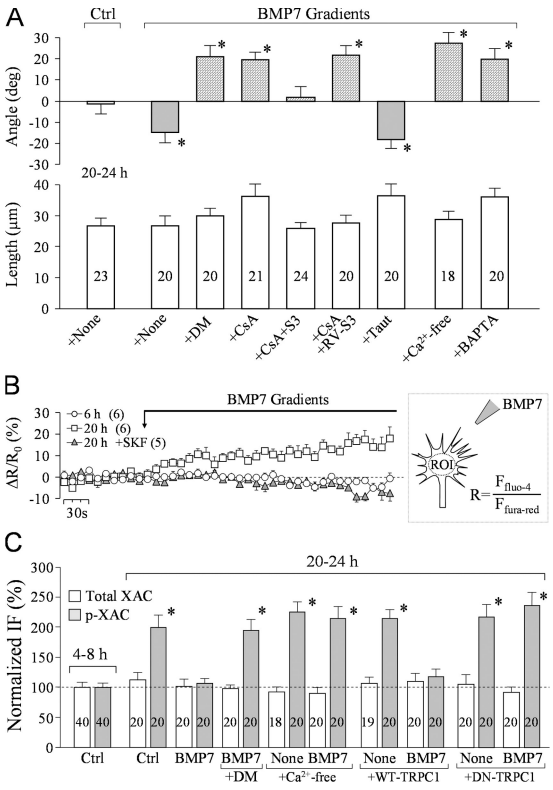

Figure 8. **BMP7-induced repulsion in overnight neurons requires Ca^{2+}–CaN signaling.** (A) Mean turning angles (top) and lengths of net extension (bottom) of different groups of growth cones examined in overnight cultures. DM, deltamethrin; CsA, cyclosporine A; Taut, tautomycin. The bars filled with a pattern show the turning responses switched from repulsion to attraction. Asterisks indicate statistical significances compared with the control (*, $P < 0.01$; Mann-Whitney test). (B) Ratiometric imaging of changes in $[Ca^{2+}]_i$ upon the onset of BMP gradients. The graph depicts the relative changes in fluo-4 and fura red ratios ($\Delta R/R_0$). The numbers in parentheses indicate the numbers of growth cones examined for each condition. 2 μM SKF96365 was added to the bath 20 min before imaging. The increase in $\Delta R/R_0$ became statistically significant 1 min after the onset of the BMP gradient ($P < 0.05$; *t* test). ROI, region of interest. (C) Normalized levels of p-XAC and XAC in *Xenopus* growth cones of 4–8-h cultures and overnight cultures with and without bath BMP7 exposure (5 nM for 10 min) under different manipulations of the Ca^{2+} signaling pathway. Asterisks indicate values that are significantly different from the control (*, $P < 0.01$; *t* test). (A and C) The numbers of growth cones examined for each condition are shown on each bar. Error bars represent SEM.

and a constitutively active (XAC3A; serine-3 replaced with alanine) or inactive (XAC3E; serine-3 replaced with glutamate) form. Expression of WT-XAC did not affect BMP7-induced attraction in 4–8-h neurons (Fig. 7 A) and repulsion in overnight cultures (Fig. 7 B). However, the overexpression of either XAC3E or XAC3A totally abolished the turning responses to BMP7 both in 4–8-h (Fig. 7 A) and overnight (Fig. 7 B) cultures. No significant effects were observed on neurite extension among these groups of growth cones ($P > 0.5$; one-way ANOVA; Fig. 7, A and B). Together with the imaging data, these findings show that BMP7 gradients elicit the asymmetric activation of LIMK1 and SSH that converge on ADF/cofilin phosphorylation to control the bidirectional responses of the growth cone.

Ca^{2+} signaling through TRPC to switch attraction to repulsion in BMP7 gradients

What caused the switching from LIMK1 activation (for attraction) to SSH activation (for repulsion) in overnight cultures? SSH could be activated by the Ca^{2+}–calmodulin-dependent phosphatase CaN (Wang et al., 2005), which is known to play a key role in Ca^{2+}-dependent growth cone repulsion (Wen et al., 2004). CaN inhibition by 10 nM of the specific inhibitors cyclosporin or deltamethrin not only abolished repulsion but converted it to LIMK-dependent attraction (Fig. 8 A). However, inhibition of phosphatase-1 by 4 nM tautomycin did not affect BMP7-induced repulsion (Fig. 8 A). CaN is activated by small Ca^{2+} signals (Rusnak and Mertz, 2000; Hudmon and Schulman, 2002); thus, we tested the involvement of Ca^{2+} signals by either removing extracellular Ca^{2+} using a Ca^{2+}-free solution or intracellular loading of *Xenopus* neurons with BAPTA to buffer the changes in $[Ca^{2+}]_i$. We found that the Ca^{2+}-free or BAPTA treatment caused the growth cones in overnight cultures to respond to BMP7 gradients with marked attraction (Fig. 8 A). This result confirms that Ca^{2+} signaling through CaN and SHH mediates BMP7-induced repulsion. We next performed ratiometric Ca^{2+} imaging and found that *Xenopus* growth cones in overnight cultures responded to the BMP7 gradient with a small but substantial increase in $[Ca^{2+}]_i$, whereas the growth cones of 6-h neurons did not show any increase in $[Ca^{2+}]_i$ (Fig. 8 B). The Ca^{2+} involvement in BMP7 effects on overnight neurons was further confirmed by the findings that the BMP7-induced decrease of p-XAC in overnight growth cones was completely abolished by CaN inhibition or by Ca^{2+}-free or BAPTA treatment (Fig. 8 C). Thus, it is conceivable that the BMP7 gradient elicits small asymmetric Ca^{2+} increases to activate CaN, which, in turn, acts on SSH to induce repulsion. Indeed, a small asymmetric elevation of $[Ca^{2+}]_i$ was observed in some overnight growth cones

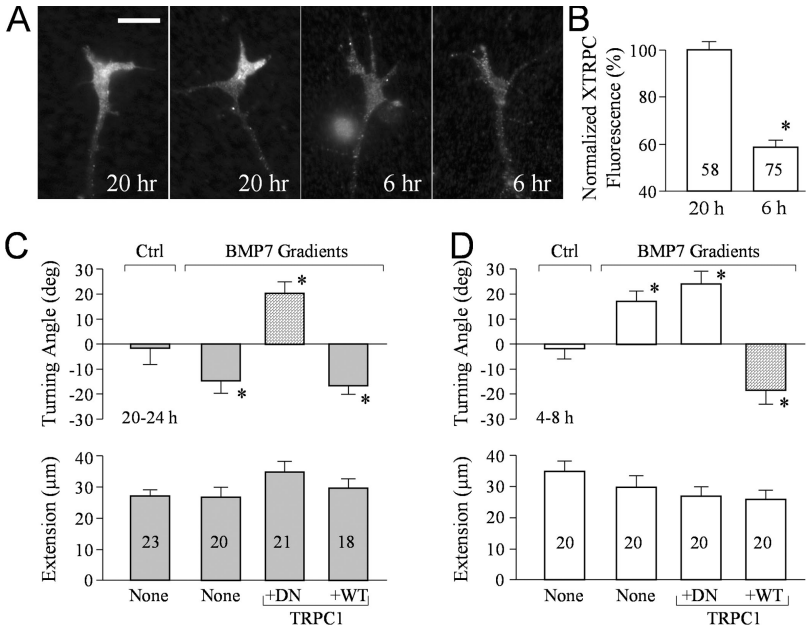

Figure 9. ***Xenopus* TRPC1 coupling the Ca^{2+}–CaN–SSH pathway to BMP7 signaling for growth cone repulsion.** (A) Representative fluorescence images of 6- or 20-h cultured *Xenopus* growth cones stained with a specific antibody against *Xenopus* TRPC1. (B) Normalized levels of *Xenopus* TRPC1 expression in *Xenopus* growth cones of 6- and 20-h cultures. The asterisk indicates statistical significance (*, $P < 0.01$; *t* test). (C and D) Mean turning angles (top) and lengths of net extension (bottom) of different groups of growth cones examined in overnight cultures (C) and 4–8-h cultures (D). The bars filled with a pattern show the turning responses switched from the original one (repulsion to attraction in overnight cultures and attraction to repulsion in 4–8-h cultures). Asterisks indicate significant differences from the corresponding control (*, $P < 0.01$ compared with the control). (B–D) The numbers of growth cones examined in each condition are shown on the bars. Error bars represent SEM. Bar, 10 μm.

upon onset of the BMP7 gradient (Fig. S3, available at http://www.jcb.org/cgi/content/full/jcb.200703055/DC1).

Recent studies show that TRP channels play an important role in growth cone guidance (Li et al., 2005; Shim et al., 2005; Wang and Poo, 2005). TRPC has been shown to interact with the carboxy-terminal tail domain of BMPRII (Hassel et al., 2004), and BMP7-induced small Ca^{2+} elevation in overnight growth cones was eliminated by 2 μM of the TRP channel inhibitor SKF96365 (Fig. 8 B). To further examine the role of TRPC, we expressed either DN-TRPC1 (phenylalanine 561 replaced with alanine) or WT-TRPC1. We found that DN- but not WT-TRPC1 abolished the BMP7-induced reduction of p-XAC, indicating that TRPC1 is involved in the BMP7-induced dephosphorylation of XAC (Fig. 8 C). Therefore, Ca^{2+} signals from TRPC1 are likely responsible for the activation of CaN and SSH to induce XAC dephosphorylation for repulsion.

Because Ca^{2+}–CaN–SSH signaling was only involved in overnight neurons for repulsive guidance by BMP7, the mechanism for generating Ca^{2+} signals likely developed between 8 and 20 h in culture. Using quantitative IF of *Xenopus* TRPC1, we found that *Xenopus* TRPC1 was expressed at a much higher level on the surface of *Xenopus* growth cones in overnight cultures compared with 4–8-h cultures (Fig. 9, A and B). This difference in the level of *Xenopus* TRPC1 on the growth cone provides an attractive model in which *Xenopus* TRPC expression may enable BMP7 to elicit Ca^{2+} signaling for CaN–SSH activation to initiate growth cone repulsion in overnight neurons, whereas 4–8-h cultures responded to BMP7 with Ca^{2+}-independent LIMK1-mediated attraction. In support of this model, the expression of DN-TRPC1 abrogated BMP7-induced repulsion and, importantly, switched it to attraction (Fig. 9 C). On the other hand, WT-TRPC1 expression did not affect the repulsion induced by BMP7 in overnight cultures. Furthermore, the overexpression of WT- but not DN-TRPC1 in 4–8-h neurons enabled consistent repulsion in the BMP7 gradient, which is a switch from the original attraction (Fig. 9 D). Therefore, these findings strongly support our hypothesis that the late emergence of TRPC1 on growth cones of overnight cultures couples BMP7 signaling to the Ca^{2+}–CaN–SSH pathway for repulsion and demonstrate that TRPCs play a crucial role in regulating the balance of phosphorylation and dephosphorylation of ADF/cofilin to control distinct turning responses by the guidance signal BMP7 at different developmental stages.

Discussion

BMPs represent one of the three families of classic morphogens that have recently been shown to guide developing axons (Charron and Tessier-Lavigne, 2005). In this study, we used cultured *Xenopus* spinal neurons and the turning assay to dissect the signaling cascades involved in BMP guidance. We find that BMP7 can act as a bidirectional guidance molecule to induce attractive and repulsive turning responses of *Xenopus* growth cones. Importantly, our study has elucidated the downstream mechanisms that control the bidirectional responses of the growth cone (Fig. 10): BMP7 attracts growth cones through the LIMK pathway (4–8-h cultures) but repels growth cones through the CaN–SSH phosphatases pathway (overnight cultures). Our data further identify ADF/cofilin as the common downstream target of these two signaling pathways to locally regulate the actin cytoskeleton for distinct turning responses: local phosphorylation (inactivation) of ADF/cofilin by LIMK leads to attraction, whereas dephosphorylation (activation) of ADF/coflin by SSH results in repulsion. Finally, we find that the key trigger for the switching of BMP7-induced attraction to repulsion is the emerging TRP channels on the growth cone membrane of overnight neurons, which enable BMP7-induced Ca^{2+} signals to activate CaN and, subsequently, SSH.

Although BMP7 repulsion has been shown for commissural axons in vivo (Augsburger et al., 1999; Butler and Dodd, 2003), it remains to be examined whether BMP7-induced attraction plays a role in axon guidance in vivo. Our real-time

PCR analysis of the expression of TRPC1 and BMPRII shows that TRPC1 emerges later than BMPRII, and it correlates with the ventral projection of commissural axons (Fig. S4, available at http://www.jcb.org/cgi/content/full/jcb.200703055/DC1). Therefore, the observed delayed emergence of TRPC1 in cultured *Xenopus* neurons is unlikely to be an artifact. Because ADF/cofilin regulation by LIMK1 is important for neurite outgrowth (Hsieh et al., 2006; Endo et al., 2007), BMP7 signaling through LIMK1 may play a role in commissural axon initiation and outgrowth in the early stage of development. The subsequent appearance of TRPC1 would then enable the commissural repulsion by BMP7 from the roof plate and, at the same time, the attraction by netrin-1 from the floor plate. Indeed, TRPC involvement in netrin-1–induced attraction was observed in overnight *Xenopus* spinal neurons (Shim et al., 2005; Wang and Poo, 2005), coinciding with the increased TRPC1 observed in this study. However, netrin-1–induced attraction appears to involve both TRPC and L-type Ca^{2+} channels to generate a relatively large Ca^{2+} signal (Nishiyama et al., 2003; Wang and Poo, 2005). Therefore, although TRPC is involved in both cases, BMP7 and netrin-1 could signal through distinct Ca^{2+} pathways to generate different responses. Finally, BMP7-induced attraction might also play a potential role in the initial guidance of commissural axons because BMP7 expression was also observed in a second location ventral to the roof plate (Augsburger et al., 1999). Nevertheless, our findings from the cultured cells have illustrated an intriguing and complex pattern of signal transduction elicited by BMP molecules that involves signal divergence and convergence. The remarkable ability of TRPC to tilt the balance to favor SSH-mediated repulsion indicates a novel role for TRP channels in influencing specific growth cone responses and further substantiates the importance of TRPC in guidance signaling.

BMP signaling through BMPRII and BMPRI is linked to the Smad activation for transcription regulation, leading to neuronal differentiation (Feng and Derynck, 2005; Liu and Niswander, 2005). We present evidence that the guidance effects are independent of the Smad pathway and selectively associated with BMPRII. In particular, BMP7 guidance was abolished by the short form BMPRII lacking the carboxy tail, which is not required for BMP activation of the Smad pathway (Ishikawa et al., 1995; Nishihara et al., 2002). It has been shown that LIMK1 interacts with this tail domain of BMPRII directly, and this interaction is required for its activation induced by BMPs (Foletta et al., 2003; Lee-Hoeflich et al., 2004; Eaton and Davis, 2005). LIMK1 regulates the actin cytoskeleton through its phosphorylation and inactivation of ADF/cofilin and has been implicated in neuronal development, including dendritogenesis, synaptic stability, and growth cone motility (Scott and Olson, 2007). Our data indicate that LIMK1 mediates growth cone attraction induced by the BMP7 gradient in the 4–8-h neurons. This conclusion is based on the results from an extensive set of experiments involving pharmacological and molecular manipulations of LIMK in conjunction with quantitative fluorescent imaging of ADF/cofilin phosphorylation and turning assays. Our live imaging of the actin cytoskeleton in 4–8-h growth cones also indicates a locally enhanced protrusion of actin-based lamellipodia and filopodia upon the onset of the BMP7 gradient. Together, these findings support a model in which the BMP7 gradient induces growth cone attraction by eliciting asymmetric actin polymerization/stabilization through the spatial regulation of ADF/cofilin activity via LIMK1. Exactly how BMP7 activates LIMK1 is still unclear. Although interaction with BMPRII is required for LIMK1 activation induced by BMP7, LIMK1 can be activated by the Rho GTPase effectors Rho kinase (Rho-associated coil-containing protein kinase [ROCK]) and p21-activated kinases (Scott and Olson, 2007). Considering the crucial role for Rho GTPases in regulating the actin cytoskeleton, it is plausible that Rho GTPases may participate in and contribute to BMP7 signaling during growth cone attraction. Furthermore, their linkage to virtually all receptors that mediate growth cone turning (Song and Poo, 2001) suggests that attractive guidance cues might all have a final common target in ADF/cofilin, which serves to integrate multiple environmental signals into a single growth cone response.

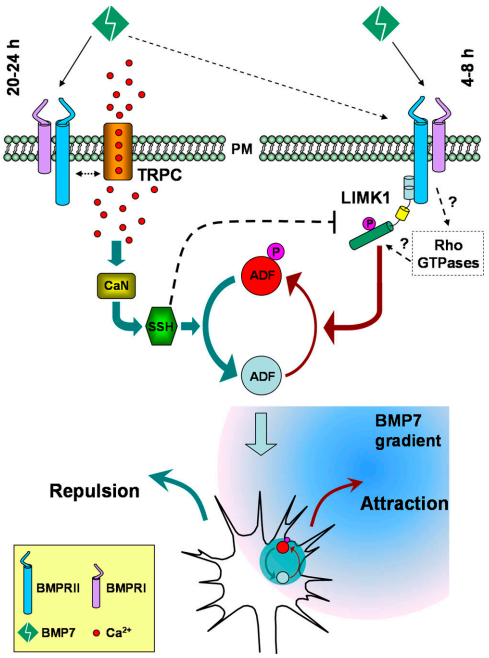

Figure 10. **Schematic diagram illustrating the signaling mechanisms that control the bidirectional responses of the growth cone to BMP7 gradients.** In 4–8-h neurons, BMP7 induces an attractive response through the LIMK pathway. In overnight neurons, BMP7 repels the growth cone through the CaN–SSH phosphatase pathway, which is activated by Ca^{2+} signaling through TRP channels. ADF/cofilin acts as the common downstream target of these two signaling pathways to locally regulate the actin cytoskeleton for distinct turning responses. PM, plasma membrane.

Our data indicate that BMP7-induced repulsion in overnight neurons is mediated by the SSH phosphatase, which is activated by Ca^{2+} signaling through CaN. This conclusion is again supported by a large set of experiments involving Ca^{2+} imaging and pharmacological and molecular manipulations of Ca^{2+}, CaN, and SSH. Importantly, the inhibition of CaN or SSH by pharmacological and molecular manipulations not only blocked BMP7-induced repulsion but consistently switched it to attraction in the overnight neurons. Furthermore, blockade of Ca^{2+} signaling also converted the repulsion to attraction in

overnight cultures (Fig. 8). These results not only indicate a key role for Ca^{2+}–CaN–SSH signaling in BMP7-induced repulsion but also demonstrate that LIMK1 can be activated in overnight neurons, although activated SSH predominates. SSH dephosphorylates ADF/cofilin at serine-3 to reactivate its actin-severing activity, and our quantitative IF shows that BMP7 induces ADF/cofilin dephosphorylation in overnight neurons, supporting the notion that BMP7 induces repulsion through the local SSH-dependent dephosphorylation of ADF/cofilin. It is notable that neurons from the overnight cultures exhibit a higher level of phospho-ADF/cofilin than those in 4–8-h cultures. Although the underlying mechanisms are unknown, such a difference in the phospho-ADF/cofilin level may reflect a difference in the actin dynamics and/or architecture in these neurons. For example, dynamic actin cytoskeleton in motile growth cones of 4–8-h neurons may undergo rapid turnover, which may involve the ADF/cofilin-severing activity (da Silva and Dotti, 2002). Alternatively, there are factors other than phosphorylation that affect ADF/cofilin activity, and these may also change during development to maintain actin dynamics. Among these factors are levels of phosphatidylinositol-4-phosphate and phosphatidylinositol-4,5-bis phosphate, pH, and tropomyosin (Bamburg and Wiggan, 2002).

The key molecule triggering the switching of attraction to repulsion appears to be TRPC1 channels. TRPC is involved in Ca^{2+}-dependent guidance by netrin-1, brain-derived neurotrophic factor, and myelin-associated glycoprotein in vitro and in vivo (Li et al., 2005; Shim et al., 2005; Wang and Poo, 2005). How these guidance molecules activate TRPCs remains unclear. A recent study found that TRPC can interact with the carboxy-terminal tail domain of BMPRII, suggesting a potential role of TRPC in the BMP7 signaling pathway (Hassel et al., 2004). The elimination of BMP-induced repulsion and XAC dephosphorylation by the short form BMPRII suggests the importance of the carboxy tail in repulsive signaling. Future experiments are clearly required to dissect the molecular mechanisms of how BMPRII interacts with and activates TRPCs. Nonetheless, our findings indicate that the switching of BMP7-induced attraction to repulsion is a result of an elevated level of TRPC1 on the growth cone surface of overnight *Xenopus* cultures.

Our model for BMP-induced bidirectional turning responses is as follows (Fig. 10): at the early stage of culture (4–8 h), BMP7 acts through BMPRII to mainly activate LIMK to asymmetrically phosphorylate ADF/cofilin for attraction. By 20–24 h in culture, a substantial amount of TRPC1 emerges on the growth cone surface, and BMPRII-TRPC coupling allows BMP7 to elicit Ca^{2+} signaling to act on CaN and SSH for repulsion. Whereas LIMK1 can still be activated by BMP7 in overnight cultures, the Ca^{2+}–CaN–SSH activation predominates for repulsion. This dominant effect could be caused by the ability of active SSH to dephosphorylate and inactivate LIMK1 (Soosairajah et al., 2005) in addition to activating ADF/cofilin. In support of this possibility, the overexpression of WT-SSH was found to attenuate BMP7-induced LIMK-dependent attraction in 4–8-h cultures (Fig. S5, available at http://www.jcb.org/cgi/content/full/jcb.200703055/DC1). Thus, this model indicates that a balancing act of LIMK1 and CaN–SSH on ADF/cofilin phosphorylation controls specific turning responses. Two crucial sets of evidence support the aforementioned model. First, in the overnight cultures, inhibition of TRPC1 by expressing DN-TRPC1 not only blocked the repulsion but also switched it back to LIMK1-dependent attraction, similar to the switching from the inhibition of Ca^{2+} signals, CaN, or SSH. Second, in the 4–8-h neurons that exhibit little TRPC1, the overexpression of WT-TRPC1 enabled the growth cones to respond to BMP7 with repulsion, confirming that TRPC1 expression is the key for BMP7-induced repulsion.

ADF/cofilin family proteins are key regulators of the actin cytoskeleton and can increase the rate of dissociation of ADP-actin from the pointed end of actin filaments and generate new filament ends through severing actin filaments (Bamburg, 1999; Gungabissoon and Bamburg, 2003). Furthermore, the severing and enhanced depolymerization are counteracted by an enhanced stabilization of actin at a high ADF/cofilin to actin ratio (Andrianantoandro and Pollard, 2006), providing for exquisite spatial and temporal control of actin dynamics. Previous studies have shown that ADF/cofilin is involved in regulating growth cone motility, morphology, and neurite extension in response to extracellular signaling molecules, including brain-derived neurotrophic factor, semaphorin 3A, and myelin-associated inhibitors (Meberg and Bamburg, 2000; Aizawa et al., 2001; Endo et al., 2003; Gehler et al., 2004; Hsieh et al., 2006). However, our findings here indicate a detailed molecular cascade that links extracellular guidance signals to intracellular cytoskeletal dynamics through phosphoregulation of ADF/cofilin activity. Furthermore, the inhibition of both attraction and repulsion by mutating the serine-3 of XAC to either alanine (XAC3A) or glutamate (XAC3E) indicates that spatial phosphoregulation of ADF/cofilin activity, not just the activity itself, is key for directional responses of growth cones to BMP7 gradients. The global presence of constitutive active (3A) or DN (3E) ADF/cofilin is likely to override any local regulation of ADF/cofilin activity elicited by BMP7 gradients, thus abolishing both turning responses. At this moment, we do not know whether local synthesis of ADF/cofilin plays a role in BMP7 guidance. Cofilin is one of the molecules whose mRNA has been detected in growth cones (Piper et al., 2006), and local synthesis of cofilin appears to be involved in Slit-2–induced growth cone collapse. BMP molecules could signal through TGFβ1-activated tyrosine kinase 1 (a MAPK kinase kinase) and MAPK (Yamaguchi et al., 1999; Liu and Niswander, 2005), which could regulate local protein synthesis. Nevertheless, even locally synthesized ADF/cofilin will be subjected to the same phosphoregulation for its effects on actin dynamics.

In summary, our study has provided important mechanistic insights into the BMP7 guidance of nerve growth cones. Specifically, our data present evidence that two distinct signaling pathways, LIMK1 and Ca^{2+}–CaN–SSH, elicited by the BMP7 gradients control attractive and repulsive growth cone responses, respectively, through a balancing act on the phosphorylation and dephosphorylation of ADF/cofilin to regulate the actin motility. A similar balancing act of kinase and phosphatase in controlling growth cone steering has also been observed for Ca^{2+} -dependent bidirectional turning (Wen et al., 2004).

It is conceivable that spatial regulation of the balance of phosphorylation and dephosphorylation of molecules involved in motility may represent a common scheme for directional responses of growth cones (Gomez and Zheng, 2006). Loss of LIMK1 has been linked to William's syndrome, a disorder characterized by visuospatial defects and mild mental retardation (Morris and Mervis, 2000). Because the loss of LIMK1 has been linked to synaptic deficits (Meng et al., 2002), it would be interesting to see whether defects in LIMK1, SSH, or ADF/cofilin may contribute to the wiring abnormality and mental retardation in William's syndrome and other neurological diseases.

Materials and methods

Xenopus embryo injection

Blastomere injections of mRNA molecules encoding different proteins into *Xenopus* embryo were performed as described previously (Alder et al., 1995; Shim et al., 2005). The DNA constructs used for mRNA preparation were provided by the following laboratories: WT and DN *Xenopus* BMPRII (provided by C. Wright, Vanderbilt University, Nashville, TN), human short form of BMPRII (provided by J. Massague, Memorial Sloan-Kettering Cancer Center, New York, NY), human WT LIMK1 and its mutant forms (provided by G. Bokoch, The Scripps Research Institute, La Jolla, CA), *Xenopus* SSH and its mutant forms (provided by H. Abe, Chiba University, Chiba, Japan), XAC or its mutant forms (Meberg and Bamburg, 2000), and human TRPC1 or its mutant forms (Shim et al., 2005). In brief, mRNA of each construct was prepared using the mMESSAGE mMACHINE kit (Ambion), and 2–3 ng was microinjected into one blastomere of *Xenopus* embryos at the one- or two-cell stage together with 10 mg/ml of fixable FITC-dextran as the marker. Injected embryos were screened for their fluorescence and used later for biochemical assays or cell cultures.

Cell culture

Embryonic *Xenopus* spinal neurons isolated from stage 20–22 *Xenopus* embryos were cultured on glass coverslips coated with poly-D-lysine and laminin as described previously (Guirland et al., 2003). The cultures were kept at 20–22°C in a serum-free medium (SFM) containing 50% (vol/vol) Leibovitz L-15 medium (Invitrogen), 50% (vol/vol) Ringer's solution (115 mM KCl, 2 mM $CaCl_2$, 2.6 mM KCl, and 10 mM Hepes, pH 7.4), and 1% (wt/vol) BSA (Sigma-Aldrich).

Growth cone turning induced by extracellular guidance gradients

Growth cone turning induced by BMP7 or BMP2 gradients was performed at room temperature according to the method described previously (Guirland et al., 2003), except assays were performed in a modified Ringer's solution (Ming et al., 1999). Microscopic gradients of chemicals were produced by the pipette application method described previously (Lohof et al., 1992; Zheng et al., 1994). A standard pressure pulse of 3 pounds per square inch was applied to a glass pipette (1-μm opening) at a frequency of 2 Hz with a pulse duration of 20 ms. The direction of growth cone extension at the beginning of the experiment was defined by the distal 20-μm segment of the neurite. The pipette tip was positioned 45° from the initial direction of extension and 100 μm away from the growth cone. With these settings, the growth cone is estimated to receive ~1/1,000th of the concentration of the tested molecule in the pipette and an ~10% relative concentration difference across the surface (Lohof et al., 1992; Zheng et al., 1994). We typically used a 20× NA 0.45 dry objective for microscopy and imaging during the turning assay. The digital images of the growth cone at the onset and end of the 30-min period were acquired by a CCD camera (C2400; Hamamatsu) and saved onto the hard drive. The images were then overlaid with pixel to pixel accuracy, and the trajectory of new neurite extension was traced using Photoshop (Adobe). The turning angle was defined by the angle between the original direction of neurite extension and a line connecting the positions of the growth cone at the experiment onset and at the end of 30-min exposure to the gradient. Neurite extension was quantified by measuring the entire trajectory of net neurite growth over the 30-min period. Only growth cones extending 5 μm or more were scored for turning responses. We used the nonparametric Mann-Whitney test to analyze turning angles because they do not follow a normal distribution.

Recombinant human BMP7 and BMP2 proteins and their antagonists follistatin (2 μg/ml) and noggin (500 ng/ml) were purchased from R&D Systems. Most of the chemical agonists and antagonists were purchased from Calbiochem. Typically, different agonists and antagonists were added to the bath medium 20 min before the onset of turning assays. The S3 and RV-S3 peptides were synthesized by GenScript containing the amino-terminal unique phosphorylation site of XAC (MASGVMVSDDVVKVFN) and were synthesized in reverse order for the RV-S3 peptide as well as a penetratin sequence (RQIKIWFQNRRMKWKK) that allowed the peptide to be internalized from the cell culture medium (Prochiantz, 1996). BAPTA was used to buffer any changes in intracellular Ca^{2+} concentrations. In brief, *Xenopus* cultures were incubated with 1 μM BAPTA-acetoxymethyl ester (Sigma-Aldrich) for 30 min, rinsed three times, and incubated with fresh SFM for 90 min before turning assays. To prevent Ca^{2+} influx, a Ca^{2+}-free solution based on Ringer's saline (115 mM KCl, 2.6 mM KCl, 2 mM $MgCl_2$, 1 mM EGTA, and 10 mM Hepes, pH 7.4) was used to replace the culture medium.

Double turning assays on the same growth cone

Xenopus neurons were plated on poly-D-lysine– and laminin-coated 18 × 18-mm^2 square coverslips with etched grids and labels (Bellco Biotechnology). The cells were cultured in SFM, and the first round of turning assays was performed in modified Ringer's solution at 4–8 h after plating as described in the previous section. The location of the cell was noted by the etched grids and labels. Afterward, the Ringer's solution was replaced by fresh SFM containing 100 U/ml penicillin and 0.1 mg/ml streptomycin, and the cells were cultured overnight for the second round of turning assays. The same neuron and its growth cone were identified by its location and verified by its morphology using the image acquired before. Quantification of the turning angles and lengths of extension was performed as described in the previous section.

Quantitative immunofluorescent imaging of phospho-ADF/cofilin, total XAC, and *Xenopus* TRPC1

Xenopus cultures with different treatments were exposed to 5 nM of bath BMP7 or to a control solution for 10 min. The cells were then rapidly fixed with 4% PFA and 0.25% glutaraldehyde in a cacodylate buffer (0.1 M sodium cacodylate and 0.1 M sucrose, pH 7.4) for 30 min, washed three times in 100% Ringer's saline, and permeabilized with 0.1% Triton X-100 for 10 min. The cells were first incubated with 1% donkey serum to block nonspecific binding sites for 1 h at room temperature. The cells were then incubated with a polyclonal antibody against phospho-ADF/cofilin (Santa Cruz Biotechnology, Inc.) or total XAC (Shaw et al., 2004). Both primary antibodies have been verified by Western blots for their reactivity to *Xenopus* neuronal tissues (Fig. S1 B). Afterward, the cells were labeled by Cy3-conjugated goat anti–rabbit secondary antibodies (The Jackson Laboratory). For mRNA-injected embryos, cells identified by their FITC-dextran fluorescence were used for quantification.

Fluorescent imaging was performed on an inverted microscope (TE2000; Nikon) using a 60× NA 1.4 plan Apo objective with identical settings between the control and exposed groups. Digital images were acquired with a CCD camera (SensiCam QE; Cooke Scientific) through the use of IPLab software (BD Biosciences). Background-subtracted images were analyzed by creating a region of interest that circumscribed the growth cone using ImageJ software (National Institutes of Health [NIH]). For each growth cone, the region of interest intensity was normalized to the mean from the parallel control. Data for each condition were obtained from at least two separate batches of *Xenopus* cultures on different days.

For quantitative imaging of *Xenopus* TRPC1, *Xenopus* cultures of different ages were fixed for 30 min and labeled (without permeabilization) with an antibody that recognizes the extracellular domain of *Xenopus* TRPC1 (Shim et al., 2005) followed by incubation with AlexaFluor488 donkey anti–rabbit IgG secondary antibodies (Invitrogen). Fluorescent imaging was performed as described in the previous paragraph.

Imaging of asymmetric p-XAC distribution in *Xenopus* growth cones

To detect the asymmetric distribution of p-XAC induced by BMP7 gradients, one growth cone in each dish was subjected to 5-min local BMP7 application through a micropipette (50 μm away; 45° angle) followed by rapid fixation, Triton X-100 permeabilization, and staining. The cells were first subjected to immunostaining for p-XAC or total XAC (see the previous section on staining method) with a Cy-3–conjugated secondary antibody followed by volume labeling using DTAF (20 mM for 20 min). Both p-XAC or XAC (red) and DTAF (green) fluorescence images were acquired, background subtracted, and the corrected images were divided to generate the final ratiometric image. Because only one growth cone was subjected to

the BMP7 gradient, the growth cones that were not exposed to the BMP7 gradient in the same dish were also imaged to serve as the control. We typically repeated the experiments for 10–20 dishes for each condition.

To analyze the asymmetry of p-XAC or XAC in the growth cone, we placed five equal-size boxes (typically 10 × 10 but adjusted to fit different growth cones) across the growth cone according to a previously described method (Yao et al., 2006). All of the quantitative measurements were performed on the original 16-bit images using ImageJ software (NIH).

Ratiometric Ca^{2+} imaging

Xenopus neurons were loaded with both fluo-4 and fura red using their acetoxymethyl forms (4 μM and 2 μM, respectively) for 30 min followed by three washes and 30-min recovery in the culture medium. Before the imaging, the bath medium was replaced with the modified Ringer's solution. The cells were imaged on a confocal microscope (C1; Nikon) using the 488-nm excitation of an argon laser and both photon multiplier tubes to simultaneously collect both the green (fluo-4) and red (fura red) fluorescence. The confocal microscope was equipped with an inverted microscope (TE300; Nikon), and a 60× NA 1.4 oil immersion objective (Nikon) was used. Time-lapse recording was performed on the growth cone at a rate of one pair every 10 s. Typically, 10 pairs of images were acquired before the onset of the BMP7 gradient followed by 30 pairs (5 min) of image acquisition. Background-subtracted ratiometric calculation was performed between fluo-4 and fura red images using ImageJ software (NIH). Measurements of the ratio were performed in a region of interest placed at the center of the growth cone (Fig. 8).

Online supplemental material

Fig. S1 shows PCR analysis of BMPRII expression and Western blotting of ADF/cofilin in *Xenopus* neural tube tissues. Fig. S2 shows fluorescence live imaging of GFP–γ-actin and mRFP-EB3 in *Xenopus* growth cones during attraction and repulsion. Fig. S3 shows asymmetric Ca^{2+} elevation in a *Xenopus* growth cone subjected to the BMP7 gradient in overnight neurons. Fig. S4 shows real-time PCR analysis of the expression profile of *Xenopus* TRPC1 and BMPRII in the *Xenopus* neural tube. Fig. S5 shows the attenuation of BMP7-induced attraction by overexpression of WT *Xenopus* SSH in 4–8-h cultures. Videos 1 and 2 show the dynamic distributions of the actin and microtubule cytoskeleton in a *Xenopus* growth cone during attraction (Video 1) and during repulsion (Video 2) to a BMP7 gradient. Supplemental text provides the methods used for the data in supplemental figures. Online supplemental material is available at http://www.jcb.org/cgi/content/full/jcb.200703055/DC1.

We would like to thank Dr. Renping Zhou (Rutgers University, New Brunswick, NJ) for sharing some of the DNA constructs.

This work is supported by grants from NIH to J.Q. Zheng (NS36241) and J.R. Bamburg (NS40371).

Submitted: 9 March 2007
Accepted: 8 June 2007

References

Aizawa, H., S. Wakatsuki, A. Ishii, K. Moriyama, Y. Sasaki, K. Ohashi, Y. Sekine-Aizawa, A. Sehara-Fujisawa, K. Mizuno, Y. Goshima, and I. Yahara. 2001. Phosphorylation of cofilin by LIM-kinase is necessary for semaphorin 3A-induced growth cone collapse. *Nat. Neurosci.* 4:367–373.

Alder, J., H. Kanki, F. Valtorta, P. Greengard, and M.M. Poo. 1995. Overexpression of synaptophysin enhances neurotransmitter secretion at *Xenopus* neuromuscular synapses. *J. Neurosci.* 15:511–519.

Andrianantoandro, E., and T.D. Pollard. 2006. Mechanism of actin filament turnover by severing and nucleation at different concentrations of ADF/cofilin. *Mol. Cell.* 24:13–23.

Augsburger, A., A. Schuchardt, S. Hoskins, J. Dodd, and S. Butler. 1999. BMPs as mediators of roof plate repulsion of commissural neurons. *Neuron.* 24:127–141.

Bamburg, J.R. 1999. Proteins of the ADF/cofilin family: essential regulators of actin dynamics. *Annu. Rev. Cell Dev. Biol.* 15:185–230.

Bamburg, J.R., and O.P. Wiggan. 2002. ADF/cofilin and actin dynamics in disease. *Trends Cell Biol.* 12:598–605.

Bovolenta, P. 2005. Morphogen signaling at the vertebrate growth cone: a few cases or a general strategy? *J. Neurobiol.* 64:405–416.

Butler, S.J., and J. Dodd. 2003. A role for BMP heterodimers in roof plate-mediated repulsion of commissural axons. *Neuron.* 38:389–401.

Charron, F., and M. Tessier-Lavigne. 2005. Novel brain wiring functions for classical morphogens: a role as graded positional cues in axon guidance. *Development.* 132:2251–2262.

da Silva, J.S., and C.G. Dotti. 2002. Breaking the neuronal sphere: regulation of the actin cytoskeleton in neuritogenesis. *Nat. Rev. Neurosci.* 3:694–704.

Dickson, B.J. 2002. Molecular mechanisms of axon guidance. *Science.* 298:1959–1964.

Eaton, B.A., and G.W. Davis. 2005. LIM Kinase1 controls synaptic stability downstream of the type II BMP receptor. *Neuron.* 47:695–708.

Endo, M., K. Ohashi, Y. Sasaki, Y. Goshima, R. Niwa, T. Uemura, and K. Mizuno. 2003. Control of growth cone motility and morphology by LIM kinase and Slingshot via phosphorylation and dephosphorylation of cofilin. *J. Neurosci.* 23:2527–2537.

Endo, M., K. Ohashi, and K. Mizuno. 2007. LIM-kinase and slingshot are critical for neurite extension. *J. Biol. Chem.* 282:13692–13702.

Feng, X.H., and R. Derynck. 2005. Specificity and versatility in tgf-beta signaling through Smads. *Annu. Rev. Cell Dev. Biol.* 21:659–693.

Foletta, V.C., M.A. Lim, J. Soosairajah, A.P. Kelly, E.G. Stanley, M. Shannon, W. He, S. Das, J. Massague, and O. Bernard. 2003. Direct signaling by the BMP type II receptor via the cytoskeletal regulator LIMK1. *J. Cell Biol.* 162:1089–1098.

Frisch, A., and C.V. Wright. 1998. XBMPRII, a novel *Xenopus* type II receptor mediating BMP signaling in embryonic tissues. *Development.* 125:431–442.

Gehler, S., A.E. Shaw, P.D. Sarmiere, J.R. Bamburg, and P.C. Letourneau. 2004. Brain-derived neurotrophic factor regulation of retinal growth cone filopodial dynamics is mediated through actin depolymerizing factor/cofilin. *J. Neurosci.* 24:10741–10749.

Gomez, T.M., and J.Q. Zheng. 2006. The molecular basis for calcium-dependent axon pathfinding. *Nat. Rev. Neurosci.* 7:115–125.

Guirland, C., K.B. Buck, J.A. Gibney, E. DiCicco-Bloom, and J.Q. Zheng. 2003. Direct cAMP signaling through G-protein-coupled receptors mediates growth cone attraction induced by pituitary adenylate cyclase-activating polypeptide. *J. Neurosci.* 23:2274–2283.

Gungabissoon, R.A., and J.R. Bamburg. 2003. Regulation of growth cone actin dynamics by ADF/cofilin. *J. Histochem. Cytochem.* 51:411–420.

Hassel, S., A. Eichner, M. Yakymovych, U. Hellman, P. Knaus, and S. Souchelnytskyi. 2004. Proteins associated with type II bone morphogenetic protein receptor (BMPR-II) and identified by two-dimensional gel electrophoresis and mass spectrometry. *Proteomics.* 4:1346–1358.

Heredia, L., P. Helguera, S. de Olmos, G. Kedikian, F. Sola Vigo, F. LaFerla, M. Staufenbiel, J. de Olmos, J. Busciglio, A. Caceres, and A. Lorenzo. 2006. Phosphorylation of actin-depolymerizing factor/cofilin by LIM-kinase mediates amyloid beta-induced degeneration: a potential mechanism of neuronal dystrophy in Alzheimer's disease. *J. Neurosci.* 26:6533–6542.

Hsieh, S.H., G.B. Ferraro, and A.E. Fournier. 2006. Myelin-associated inhibitors regulate cofilin phosphorylation and neuronal inhibition through LIM kinase and Slingshot phosphatase. *J. Neurosci.* 26:1006–1015.

Hudmon, A., and H. Schulman. 2002. Neuronal CA2+/calmodulin-dependent protein kinase II: the role of structure and autoregulation in cellular function. *Annu. Rev. Biochem.* 71:473–510.

Ishikawa, T., H. Yoshioka, H. Ohuchi, S. Noji, and T. Nohno. 1995. Truncated type II receptor for BMP-4 induces secondary axial structures in *Xenopus* embryos. *Biochem. Biophys. Res. Commun.* 216:26–33.

Le Roux, P., S. Behar, D. Higgins, and M. Charette. 1999. OP-1 enhances dendritic growth from cerebral cortical neurons in vitro. *Exp. Neurol.* 160:151–163.

Lee, K.J., and T.M. Jessell. 1999. The specification of dorsal cell fates in the vertebrate central nervous system. *Annu. Rev. Neurosci.* 22:261–294.

Lee-Hoeflich, S.T., C.G. Causing, M. Podkowa, X. Zhao, J.L. Wrana, and L. Attisano. 2004. Activation of LIMK1 by binding to the BMP receptor, BMPRII, regulates BMP-dependent dendritogenesis. *EMBO J.* 23:4792–4801.

Lein, P., M. Johnson, X. Guo, D. Rueger, and D. Higgins. 1995. Osteogenic protein-1 induces dendritic growth in rat sympathetic neurons. *Neuron.* 15:597–605.

Li, Y., Y.C. Jia, K. Cui, N. Li, Z.Y. Zheng, Y.Z. Wang, and X.B. Yuan. 2005. Essential role of TRPC channels in the guidance of nerve growth cones by brain-derived neurotrophic factor. *Nature.* 434:894–898.

Liu, A., and L.A. Niswander. 2005. Signalling in development: bone morphogenetic protein signalling and vertebrate nervous system development. *Nat. Rev. Neurosci.* 6:945–954.

Lohof, A.M., M. Quillan, Y. Dan, and M.M. Poo. 1992. Asymmetric modulation of cytosolic cAMP activity induces growth cone turning. *J. Neurosci.* 12:1253–1261.

Meberg, P.J., and J.R. Bamburg. 2000. Increase in neurite outgrowth mediated by overexpression of actin depolymerizing factor. *J. Neurosci.* 20:2459–2469.

Meng, Y., Y. Zhang, V. Tregoubov, C. Janus, L. Cruz, M. Jackson, W.Y. Lu, J.F. MacDonald, J.Y. Wang, D.L. Falls, and Z. Jia. 2002. Abnormal spine morphology and enhanced LTP in LIMK-1 knockout mice. *Neuron*. 35:121–133.

Ming, G.L., H.J. Song, B. Berninger, C.E. Holt, M. Tessier-Lavigne, and M.M. Poo. 1997. cAMP-dependent growth cone guidance by netrin-1. *Neuron*. 19:1225–1235.

Ming, G., H. Song, B. Berninger, N. Inagaki, M. Tessier-Lavigne, and M. Poo. 1999. Phospholipase C-gamma and phosphoinositide 3-kinase mediate cytoplasmic signaling in nerve growth cone guidance. *Neuron*. 23:139–148.

Morris, C.A., and C.B. Mervis. 2000. Williams syndrome and related disorders. *Annu. Rev. Genomics Hum. Genet.* 1:461–484.

Nishihara, A., T. Watabe, T. Imamura, and K. Miyazono. 2002. Functional heterogeneity of bone morphogenetic protein receptor-II mutants found in patients with primary pulmonary hypertension. *Mol. Biol. Cell*. 13:3055–3063.

Nishita, M., H. Aizawa, and K. Mizuno. 2002. Stromal cell-derived factor 1alpha activates LIM kinase 1 and induces cofilin phosphorylation for T-cell chemotaxis. *Mol. Cell. Biol.* 22:774–783.

Nishita, M., C. Tomizawa, M. Yamamoto, Y. Horita, K. Ohashi, and K. Mizuno. 2005. Spatial and temporal regulation of cofilin activity by LIM kinase and Slingshot is critical for directional cell migration. *J. Cell Biol.* 171:349–359.

Nishiyama, M., A. Hoshino, L. Tsai, J.R. Henley, Y. Goshima, M. Tessier-Lavigne, M.M. Poo, and K. Hong. 2003. Cyclic AMP/GMP-dependent modulation of Ca2+ channels sets the polarity of nerve growth-cone turning. *Nature*. 423:990–995.

Niwa, R., K. Nagata-Ohashi, M. Takeichi, K. Mizuno, and T. Uemura. 2002. Control of actin reorganization by Slingshot, a family of phosphatases that dephosphorylate ADF/cofilin. *Cell*. 108:233–246.

O'Dowd, D.K. 1983. RNA synthesis dependence of action potential development in spinal cord neurones. *Nature*. 303:619–621.

Piper, M., R. Anderson, A. Dwivedy, C. Weinl, F. van Horck, K.M. Leung, E. Cogill, and C. Holt. 2006. Signaling mechanisms underlying slit2-induced collapse of *Xenopus* retinal growth cones. *Neuron*. 49:215–228.

Prochiantz, A. 1996. Getting hydrophilic compounds into cells: lessons from homeopeptides. *Curr. Opin. Neurobiol.* 6:629–634.

Rusnak, F., and P. Mertz. 2000. Calcineurin: form and function. *Physiol. Rev.* 80:1483–1521.

Schindelholz, B., and B.F. Reber. 1999. Quantitative estimation of F-actin in single growth cones. *Methods*. 18:487–492.

Scott, R.W., and M.F. Olson. 2007. LIM kinases: function, regulation and association with human disease. *J. Mol. Med*. 85:555–568.

Shaw, A.E., L.S. Minamide, C.L. Bill, J.D. Funk, S. Maiti, and J.R. Bamburg. 2004. Cross-reactivity of antibodies to actin-depolymerizing factor/cofilin family proteins and identification of the major epitope recognized by a mammalian actin-depolymerizing factor/cofilin antibody. *Electrophoresis*. 25:2611–2620.

Shewan, D., A. Dwivedy, R. Anderson, and C.E. Holt. 2002. Age-related changes underlie switch in netrin-1 responsiveness as growth cones advance along visual pathway. *Nat. Neurosci.* 5:955–962.

Shim, S., E.L. Goh, S. Ge, K. Sailor, J.P. Yuan, H.L. Roderick, M.D. Bootman, P.F. Worley, H. Song, and G.L. Ming. 2005. XTRPC1-dependent chemotropic guidance of neuronal growth cones. *Nat. Neurosci.* 8:730–735.

Song, H., and M. Poo. 2001. The cell biology of neuronal navigation. *Nat. Cell Biol.* 3:E81–E88.

Soosairajah, J., S. Maiti, O. Wiggan, P. Sarmiere, N. Moussi, B. Sarcevic, R. Sampath, J.R. Bamburg, and O. Bernard. 2005. Interplay between components of a novel LIM kinase-slingshot phosphatase complex regulates cofilin. *EMBO J.* 24:473–486.

Stoop, R., and M.M. Poo. 1995. Potentiation of transmitter release by ciliary neurotrophic factor requires somatic signaling. *Science*. 267:695–699.

Tanaka, K., R. Nishio, K. Haneda, and H. Abe. 2005. Functional involvement of *Xenopus* homologue of ADF/cofilin phosphatase, slingshot (XSSH), in the gastrulation movement. *Zoolog. Sci.* 22:955–969.

Tessier-Lavigne, M., and C.S. Goodman. 1996. The molecular biology of axon guidance. *Science*. 274:1123–1133.

Wang, G.X., and M.M. Poo. 2005. Requirement of TRPC channels in netrin-1-induced chemotropic turning of nerve growth cones. *Nature*. 434:898–904.

Wang, Y., F. Shibasaki, and K. Mizuno. 2005. Calcium signal-induced cofilin dephosphorylation is mediated by Slingshot via calcineurin. *J. Biol. Chem.* 280:12683–12689.

Wen, Z., C. Guirland, G.L. Ming, and J.Q. Zheng. 2004. A CaMKII/calcineurin switch controls the direction of Ca(2+)-dependent growth cone guidance. *Neuron*. 43:835–846.

Yamaguchi, K., S. Nagai, J. Ninomiya-Tsuji, M. Nishita, K. Tamai, K. Irie, N. Ueno, E. Nishida, H. Shibuya, and K. Matsumoto. 1999. XIAP, a cellular member of the inhibitor of apoptosis protein family, links the receptors to TAB1-TAK1 in the BMP signaling pathway. *EMBO J.* 18:179–187.

Yamashita, H., P. ten Dijke, D. Huylebroeck, T.K. Sampath, M. Andries, J.C. Smith, C.H. Heldin, and K. Miyazono. 1995. Osteogenic protein-1 binds to activin type II receptors and induces certain activin-like effects. *J. Cell Biol.* 130:217–226.

Yao, J., Y. Sasaki, Z. Wen, G.J. Bassell, and J.Q. Zheng. 2006. An essential role for beta-actin mRNA localization and translation in Ca2+-dependent growth cone guidance. *Nat. Neurosci.* 9:1265–1273.

Yoshikawa, S., and J.B. Thomas. 2004. Secreted cell signaling molecules in axon guidance. *Curr. Opin. Neurobiol.* 14:45–50.

Zheng, J.Q., M. Felder, J.A. Connor, and M.M. Poo. 1994. Turning of nerve growth cones induced by neurotransmitters. *Nature*. 368:140–144.

Zimmerman, L.B., J.M. De Jesus-Escobar, and R.M. Harland. 1996. The Spemann organizer signal noggin binds and inactivates bone morphogenetic protein 4. *Cell*. 86:599–606.